

Follow-Your-Pose v2: Multiple-Condition Guided Character Image Animation for Stable Pose Control

Jingyun Xue^{1,2*}, Hongfa Wang^{2*}, Qi Tian^{2*}, Yue Ma^{2,4}, Andong Wang², Zhiyuan Zhao², Shaobo Min², Wenzhe Zhao², Kaihao Zhang³, Heung-Yeung Shum⁴, Wei Liu², Mengyang Liu^{2†}, Wenhan Luo^{1,4†}

¹Sun Yat-sen University, ²Tencent Hunyuan, ³Harbin Institute of Technology (Shenzhen), ⁴HKUST

<https://follow-your-pose-v2.github.io>

ABSTRACT

Pose-controllable character video generation is in high demand with extensive applications for fields such as automatic advertising and content creation on social media platforms. While existing character image animation methods using pose sequences and reference images have shown promising performance, they tend to struggle with incoherent animation in complex scenarios, such as multiple character animation and body occlusion. Additionally, current methods request large-scale high-quality videos with stable backgrounds and temporal consistency as training datasets, otherwise, their performance will greatly deteriorate. These two issues hinder the practical utilization of character image animation tools. In this paper, we propose a practical and robust framework Follow-Your-Pose v2, which can be trained on noisy open-sourced videos readily available on the internet. Multi-condition guiders are designed to address the challenges of background stability, body occlusion in multi-character generation, and consistency of character appearance. Moreover, to fill the gap of fair evaluation of multi-character pose animation, we propose a new benchmark comprising approximately 4,000 frames. Extensive experiments demonstrate that our approach outperforms state-of-the-art methods by a margin of over 35% across 2 datasets and on 7 metrics. Meanwhile, qualitative assessments reveal a significant improvement in the quality of generated video, particularly in scenarios involving complex backgrounds and body occlusion of multi-character, suggesting the superiority of our approach.

CCS CONCEPTS

• Computing methodologies → Computer vision.

KEYWORDS

Pose control, Video generation, Character image animation, Latent diffusion model

1 INTRODUCTION

Character image animation task targets animating a given static character image to a video clip using a sequence of motion signals, such as video, depth or pose, while preserving the visual appearance. It has attracted much attention and extensively explored in research [17, 39, 44, 48, 49, 52]. This technology has widespread applications in fields of the film industry, automatic advertising and content creation for social media platforms, *etc.* As a data-driving task, cocurrent character image animation frameworks [18, 39, 50]

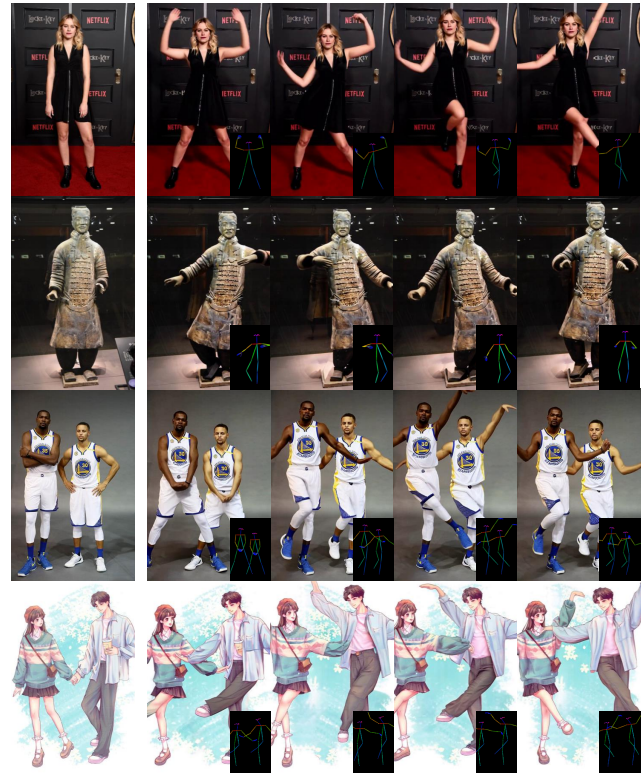


Figure 1: Pose-controllable character animation results given the leftmost reference image. The top two rows depict single-character animation results while the bottom two rows illustrate dual-character animation results.

always optimize the model on high-quality video datasets, which request stable background and temporal consistency. The expensive collection of datasets restricts their utility in more common scenarios.

Existing character image animation can be divided into two categories based on the generative mechanism: GAN-based and diffusion-based frameworks. Previous methods [32, 41] leverage a warping function to transfer the reference image into the target pose, and then GAN model is employed to generate the missing parts. In recent years, encouraged by the emergency of diffusion models [34], the models use pose condition [17] and harness appearance [44] to generate natural video clips based on pretrained stable diffusion [30]. Despite generating visually plausible video,

* These authors contributed equally to this research.

† Corresponding authors.

these methods frameworks still face several challenges. GAN-based methods fail to generate realistic character animation due to poor ability of motion transfer, such as hair, facial expressions, and other details. It becomes more serious in cross-identity scenarios. In contrast, diffusion-based methods alleviate this problem due to their powerful generative capability. However, they still synthesize incoherent animation in a frame-by-frame operation. These methods always have serious challenges in some complex pose sequences, such as multiple character pose sequences and body occluded pose sequences. Such approaches typically rely solely on pose as a condition, neglecting the benefits of considering various conditions, leading to flickering results.

In this work, to address the aforementioned limitations, we develop a general character image animation framework called *Follow-Your-Pose v2*, which employs multi-condition guided generation and optimizes our model on the large-scale noisy dataset from the internet. Specifically, we design the optical flow guider to achieve better background stability, resulting in a significant improvement. Secondly, to address the issue of occluded body parts in multiple character animation, we propose the use of the depth guider to assist the model in distinguishing between the foreground and background, thus maintaining the identification of different characters. Thirdly, the reference pose guider is proposed for better appearance learning. Finally, we collect a large number of video clips from the Internet for our training dataset. These videos encompass diverse elements such as backgrounds, clothing, races, and multiple character scenarios, all of which can enhance the generalization ability of the model. However, a notable drawback is that the majority of these videos exhibit camera shake or unstable backgrounds. Thanks to the multiple condition guiders, our framework could generate temporally consistent and realistic detailed single and multiple character image animations using noisy video clips as our training set. Additionally, to evaluate the performance of multi-pose sequence generation, we also propose a multi-pose benchmark including about 4000 frames, which empowers researchers to measure the generation ability in complex multiple character animations. To the best of our knowledge, we are the first to collect such a benchmark. We conduct plenty of quantitative and qualitative experiments to illustrate the superiority of our approach. Compared with cocurrent methods [17, 39], our approach has achieved remarkable improvements in all 7 metrics across all experiments.

In summary, our contributions are four-fold:

- We propose a practical and multi-condition guided framework *Follow-Your-Pose v2* to leverage large-scale noisy data for character image animation, which improves the performance significantly.
- To achieve efficient training using noisy data, technically, the *optical flow guider* ensures background stability, the *depth guider* addresses the occlusion among body parts, and *reference pose guider* enhances the learning of subject appearance.
- To address the lack of a benchmark in multiple character image animation, we introduce a new benchmark called *Multi-Character Bench*, which contains about 4,000 frames for fair evaluation.
- Extensive quantitative and qualitative evaluations are conducted using two public datasets and Multi-Character Bench. The experiments show the superiority of the proposed method.

2 RELATED WORK

2.1 Diffusion Models for Video Generation

Compared with aforementioned GAN-based methods [25, 33, 54], diffusion models [5, 6, 8, 10–12, 19, 21, 23, 24, 26, 34, 43, 47, 50, 51] excel in generating high-quality contents and exhibit greater training efficiency. Diffusion models were first proposed to generate images [14, 34]. Many studies adapt image synthesis pipelines for video generation [5, 6, 11, 19, 43]. Text2Video-Zero [19] incorporates motion dynamics in generated frames via cross-frame attention in zero-shot style. Animatediff [11] finetunes a plug-and-play motion module that can be integrated into any text-to-image models to obtain animations in a personalized style. VideoCrafter [5, 6] achieves both text-to-video and image-to-video generation and produces videos of high resolution. Besides text, I2V-Adapter [10] extracts semantics from images to condition T2V generation.

2.2 Pose-Controllable Character Animation

Generating realistic character video from the driving signal (e.g., key points, depth maps) has been extensively studied in recent years. Early approaches employed GAN-based models for conditional video synthesis [25, 32, 41]. Vid2vid [40] utilizes conditional GAN to produce diverse pose videos by incorporating optical flow, temporal consistency constraints, and multiple discriminators. Similar work [3] is proposed to transfer movements from a source person to a target person through keypoints. MRAA [33] extends this line of research by incorporating consistent regions that describe locations, shapes, and poses. To address the pose gap between objects in the source and driving images, TPSMM [54] effectively aligns object poses using thin-plate spline motion estimation, multi-resolution occlusion masks, and carefully designed loss functions.

With the development of diffusion model [14], existing methods incorporate pose sequences to guide the generation of the character video clips [4, 17, 18, 22, 39, 44, 44, 50]. DreamPose [18] proposes a finetuning framework to adapt the Stable Diffusion model [30] to a pose-and-image guided video synthesis model. AnimateAnyone [17] designs ReferenceNet to merge detailed human body features, ensuring character appearance consistency, while employing a pose guider and temporal modeling for controllable and continuous movements. To enhance the faithfulness, generalizability, and compositionality of character animation, DisCo [39] disentangles the control conditions (i.e., character foreground, background, and poses) by introducing multiple ControlNets for different feature embeddings and proposes a human attribute pre-training framework. Moreover, a two-stage training scheme [22] is proposed to address the lack of comprehensive paired video-pose datasets, leveraging available image pose pairs, pose-free videos, and a pre-trained text-to-image model to generate pose-controllable character videos. However, both GAN-based and diffusion-based methods fail to effectively address the issue of background stability and occlusion among body parts.

3 PRELIMINARIES

Latent Diffusion Models. The latent diffusion models [30] (LDM) performs a denoising process within the latent space rather than the image pixel space [14, 34], cutting computational load while

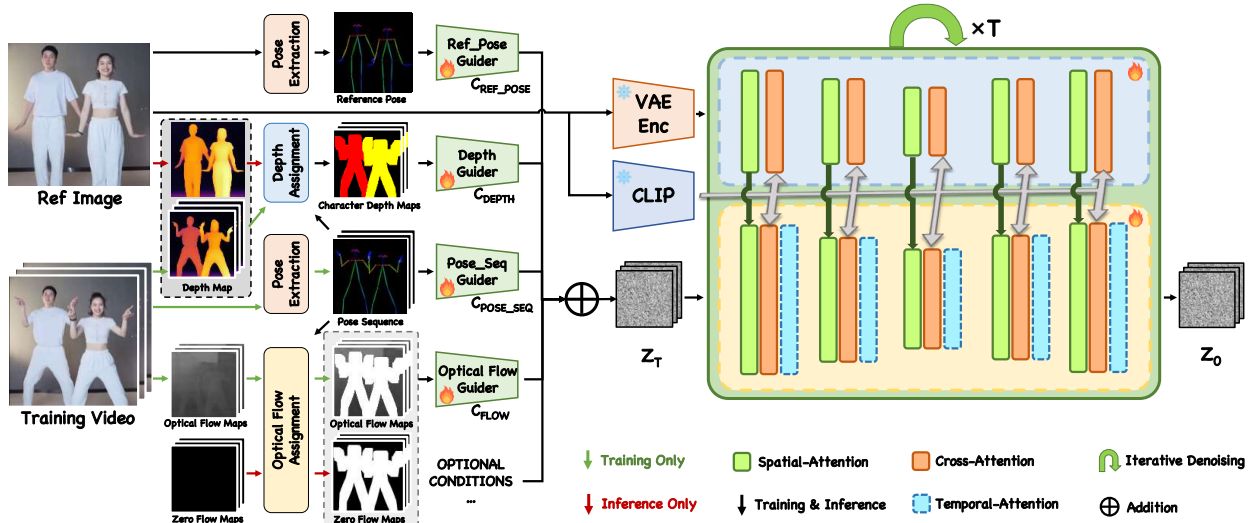


Figure 2: The overview of the proposed Follow-Your-Pose v2. The left half illustrates the data flow of the multiple condition guiders, with green and black arrows denoting training data flow, and red and black arrows indicating inference data flow. The right half shows the denoising U-Net and ReferenceNet.

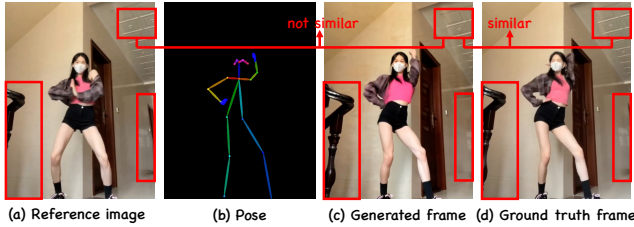


Figure 3: The result of the model trained on the background unstable dataset. The red box highlights the phenomenon where the background of the generated image deviates from that of the inference image.

maintaining quality. Specifically, the encoder of variational autoencoder [20, 29, 37] (VAE) compresses the pixel space image x to a latent space feature $z = \mathcal{E}(x)$, while the decoder reconstructs the generated latent space feature z' back into image $x' = \mathcal{D}(z')$. The denoising process is an iterative Markov process that progressively denoises the initial Gaussian noise $z_T \in \mathcal{N}(0, I)$ into the target latent space features z_0 . The single-step iterative process involves predicting the noise of the forward process and subtracting it. LDM uses U-Net [31] or Transformer [27, 38] to estimate the noise, with the loss function of

$$\mathcal{L} = \mathbb{E}_{\mathcal{E}(x), c, \epsilon \sim \mathcal{N}(0, I), t} [\|\epsilon - \epsilon_{\theta}(z^t, t, c)\|_2^2], \quad (1)$$

where $\epsilon_{\theta}(\cdot)$ is the network for predicting noise. c denotes the conditional information. t represents the timestep of denoising process and z^t represents the intermediate result of denoising at timestep t . **Temporal Motion Modules.** Video can be regarded as a sequence of moving images in the temporal dimension. Based on the powerful image generation capability of the text-to-image (T2I) model, the addition of temporal motion modules endows it with the ability to generate video [11], *i.e.*, video latent diffusion model (VLDM).

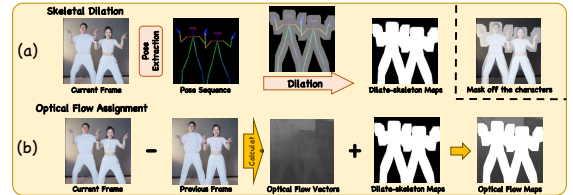


Figure 4: The pipeline of calculating the skeletal dilation map and optical flow map. The optical flow map is obtained by superimposing the skeletal dilation map onto the optical flow vector map.

Specifically, inflating the T2I model enables it to generate video data, and insert a temporal motion module after spatial attention. The temporal motion modules run across temporal frames in each batch to enhance motion smoothness and content consistency in animation clips. Besides, the initial input tensor $z \in \mathbb{R}^{c \times h \times w}$ of the T2I model should add a temporal dimension and repeat it n times, becoming $z_{1:n} \in \mathbb{R}^{n \times c \times h \times w}$. The VLDM's loss function is

$$\mathcal{L} = \mathbb{E}_{\mathcal{E}(v_{1:n}), c, \epsilon_{1:n} \sim \mathcal{N}(0, I), t} [\|\epsilon - \epsilon_{\theta}(z_{1:n}^t, t, c)\|_2^2], \quad (2)$$

where $v_{1:n}, \epsilon_{1:n}, z_{1:n}^t$ respectively represent the corresponding variables after adding dimensions in Eq. (1).

4 METHOD

Given a reference image I_0 and the pose sequences $\{P_0, P_1, P_2, \dots, P_N\}$, the primary objective is to generate character video clip not only exhibits plausible motion but also faithfully preserves the visual appearance (foreground and background) of the reference image. By leveraging large-scale high-quality dataset training, recent methods have shown promising generation capacity. However, the collection of videos with stable backgrounds is costly and laborious.

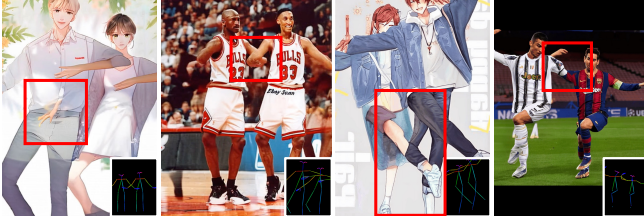


Figure 5: Bad cases of multi-character animation. The red boxes indicate the body occlusion regions of multiple characters that the model fails to generate accurately.

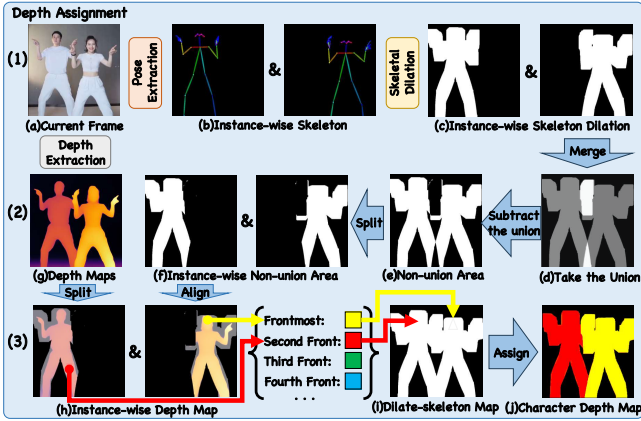


Figure 6: The pipeline of calculating the depth map. The yellow module “Skeletal Dilation” is shown in Fig. 4 (a).

Meanwhile, existing methods offer limited performance over the multi-character generation and occluded body parts. In view of these limitations, we propose Follow-Your-Pose v2 (FYPv2), a novel framework equipped the multi-condition guiders, as shown in Fig. 2. The **optical flow guider**, detailed in Sec. 4.1, focuses on the stability control of the background. The **depth guider**, described in Sec. 4.2, tackles the occlusion of pose sequences in multi-character animation. We also present the details about the designed **reference pose guider** in Sec. 4.3. Finally, the base model architecture and objective loss are introduced in Sec. 4.4.

4.1 Optical flow guider

Directly optimizing the model on a noisy dataset results in background instability, which may be attributed to training data with an unstable background. As shown in Fig. 3, we present the generated video frames during the training stage. It is clear that the model tends to generate dynamic backgrounds similar to the ground truth rather than the reference image. This is a common issue when training on noisy datasets. To deal with this problem, we utilize the guidance of optical flow to achieve stable background generation. Fig. 4 presents the pipeline of calculating the optical flow map in the training stage [7, 9, 35, 46]. The optical flows from each frame $\{x_1, x_2, \dots, x_N\}$ are predicted by open-source optical flow estimator \mathcal{E}_{flow} [7]. The dilation operation is then applied on pose skeletons to obtain binary mask sequences $\{\mathcal{M}_1, \mathcal{M}_2, \mathcal{M}_3, \dots, \mathcal{M}_N\}$, which

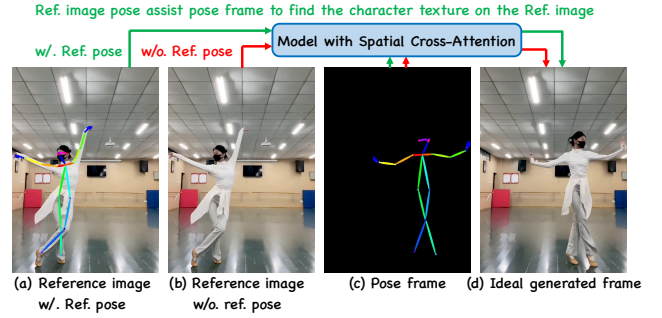


Figure 7: The potential impact of inputting reference image pose for model generation.

are used for definition of the control region. We blend optical flows with the binary mask and encode them using 8 layer inflated 3D convolution. Following the animate anyone [17], the representations are added into clear initial noise latent. In inference stage, the region in blended optical flows is set to 1.0. Formally, the optical flow guider is implemented as

$$\mathcal{M}_i = \mathcal{D}(P_i),$$

$$c_{flow}^i = (1 - \mathcal{M}_i) \odot \mathcal{E}_{flow}(x_i) \quad (3)$$

where $i = 1, 2, 3, \dots, N$, \mathcal{D} is the dilation operation, \mathcal{E}_{flow} represents the optical flow estimator, \odot represents Hadamard product.

4.2 Depth guider

Cocurrent methods struggle to process scenarios with body occlusion. Insufficient understanding of spatial relations renders these methods incapable of accurately generating occluded body parts, as illustrated by the red boxes in Fig. 5. The reason is that the absence of spatial information within the pose sequence results in various body occlusions mapping to the same pose frame, rendering the model incapable of learning the correct spatial relationships between foreground and background.

To solve this problem, we develop incorporating the depth map as a condition within the proposed framework [45]. The aim is to leverage the spatial information in the depth maps to assist the model in learning spatial relationships between characters. Fig. 6 illustrates the pipeline for incorporating the depth maps into the proposed framework, which can be divided into three processes. The first process is indicated in the first row of Fig. 6. For the current frame, we extract the pose of each character individually, and then apply “Skeletal Dilation” (See Fig. 4 (a)) to each of them, resulting in Instance-wise Skeleton Dilation Maps, *i.e.*, Fig. 6 (c). In the second process, we first merge the (c) to take the union, and then subtract the union to get the Non-union Area. Subsequently, we split it by characters, resulting in the Instance-wise Non-union Area Maps, which represent the non-union region of each character, *i.e.*, Fig. 6 (f). Lastly, we extract Depth Maps of the current frame, *i.e.*, Fig. 6 (g). In the third process, we first split (g) by characters, and then align them with (f). Consequently, we can compute the average depth of non-union region for each character, and then sort them by the average depth to obtain their position ranking. We set a value list to assign values to the region of each character based

Table 1: Quantitative comparison on Tiktok Dataset. The best and second-best results are indicated in red and blue respectively.

Method	FID↓	SSIM↑	PSNR↑	LPIPS↓	L1↓	FID-VID↓	FVD↓
MRAA[33]	54.47	0.672	29.39	0.296	3.21E-04	66.36	284.82
TPSMM[54]	53.78	0.673	29.18	0.299	3.23E-04	72.55	306.17
DreamPose[18]	79.46	0.509	28.04	0.450	6.91E-04	80.51	551.56
DisCo[39]	51.29	0.699	28.70	0.333	1.10E-04	61.41	379.56
DisCo+[39]	48.29	0.713	28.78	0.320	1.03E-04	52.56	334.67
MagicAnimate[44]	32.09	0.714	29.16	0.239	3.13E-04	21.75	179.07
MagicPose[4]	25.50	0.752	29.53	0.292	0.81E-04	46.30	216.01
AnimateAnyone[17]	-	0.718	29.56	0.285	-	-	171.90
Ours	27.70	0.760	29.70	0.272	0.73E-04	14.30	117.81

Table 2: Quantitative comparison on TED-talks Dataset. The best and the second-best results are indicated in red and blue respectively. MRAA* and TPSMM* present these methods utilize ground-truth videos as driving signals, while gray metrics represent that they do not participate in quantitative comparisons.

Method	FID↓	SSIM↑	PSNR↑	LPIPS↓	L1↓	FID-VID↓	FVD↓
MRAA*[33]	25.76	0.807	32.62	0.216	0.36E-04	12.20	126.28
TPSMM*[54]	24.69	0.819	32.92	0.205	0.35E-04	9.04	87.76
MRAA[33]	50.36	0.762	31.90	0.266	0.50E-04	82.79	493.02
TPSMM[54]	23.71	0.771	32.30	0.252	0.49E-04	32.12	260.67
DisCo[39]	75.48	0.575	27.99	0.309	1.21E-04	66.18	393.04
DisCo+[39]	63.28	0.596	28.12	0.300	1.11E-04	55.81	343.20
MagicAnimate[44]	41.58	0.529	28.28	0.310	1.73E-04	33.61	223.54
MagicPose[4]	23.39	0.723	30.08	0.236	0.81E-04	27.53	214.23
Ours	18.21	0.779	30.88	0.198	0.46E-04	10.24	81.73

on its position ranking. For example, as shown in Fig. 6 (i), we assign “yellow value” to the frontmost character region and “red value” to the second front character region. Finally, we obtain the “character depth map”, *i.e.*, Fig. 6 (j), containing the spatial relational information we desired. Given a training video v , where the i_{th} frame is denoted as v_i , and suppose that J characters on v_i . These processes can be illustrated as

$$a_{i,1}, \dots, a_{i,J} = f_e(f_s(v_i)), \quad (4)$$

$$m_{i,j} = a_{i,j} - \left(1 - \bigcup_{j \in \{1, \dots, J\}} (a_{i,j})\right), j \in \{1..J\}, \quad (5)$$

$$rank_j = f_{\text{sort}}(m_{i,1} \odot f_d(v_1), \dots, m_{i,j} \odot f_d(v_i)), \quad (6)$$

$$c_{\text{depth},j} = m_{i,j} \odot L_{\text{rank}_j} + \left(1 - m_{i,j} \odot c_{\text{depth},(j-1)}\right), c_{\text{depth},0} = 0, \quad (7)$$

$$c_{\text{depth}} = g_{\text{dp}}(c_{\text{depth},J}), \quad (8)$$

where f_d represents the depth extraction network, $a_{i,j}$ is the instance-wise skeleton dilation map, *i.e.*, Fig. 6 (c). \cup represents union operation and $m_{i,j}$ is the non-union region of each character, *i.e.*, Fig. 6 (f). f_{sort} represents average depth sorting (descending order), $rank_j$ is the depth ranking of character j , and L_{rank_j} denotes the value assigned to j based on depth ranking. $c_{\text{depth},j}$ represents the depth map of the farthest j characters. g_{dp} represents the depth guider.

4.3 Reference pose guider

The positions of characters in inference images and pose sequences often exhibit inconsistencies. As indicated by the red arrows in Fig. 7, the model employs spatial cross-attention to facilitate the

interaction between the pose frame and reference image, enabling it to learn character texture information from the reference images and accurately map them to the corresponding pose positions. Therefore, the model is required to perceive the entirety of the reference image through spatial cross-attention in order to capture the position and texture information of the characters. This presents a significant learning challenge for the model.

We realize that this process involves the model implicitly learning character poses in the reference image and aligning them with the pose frame. Consequently, we can address this issue by introducing the reference pose as a prior. The green arrows in Fig. 6 show that the reference pose serves as a prior, to assist the model in accurately locating the character on the reference image. In this way, the model can efficiently accomplish mapping by focusing on the area specified by the reference pose within the spatial cross-attention. Besides, since the reference pose map and the pose frame are consistent in format, the model can directly align the pose and map the characters efficiently. Given the reference image x , the $c_{\text{ref_pose}}$ can be formulated as

$$c_{\text{ref_pose}} = g_{\text{rp}}(f_s(x)), \quad (9)$$

where f_s represents the skeleton extraction network and g_{rp} denotes the reference pose guider.

4.4 Base Model Architecture

As is shown in Fig. 2. FYPv2 contains some modules that are widely used in the pose-guided animation community. Specifically, the reference image is compressed using VAE and then fed into referencenet [2]. It interacts with the features in the U-net model

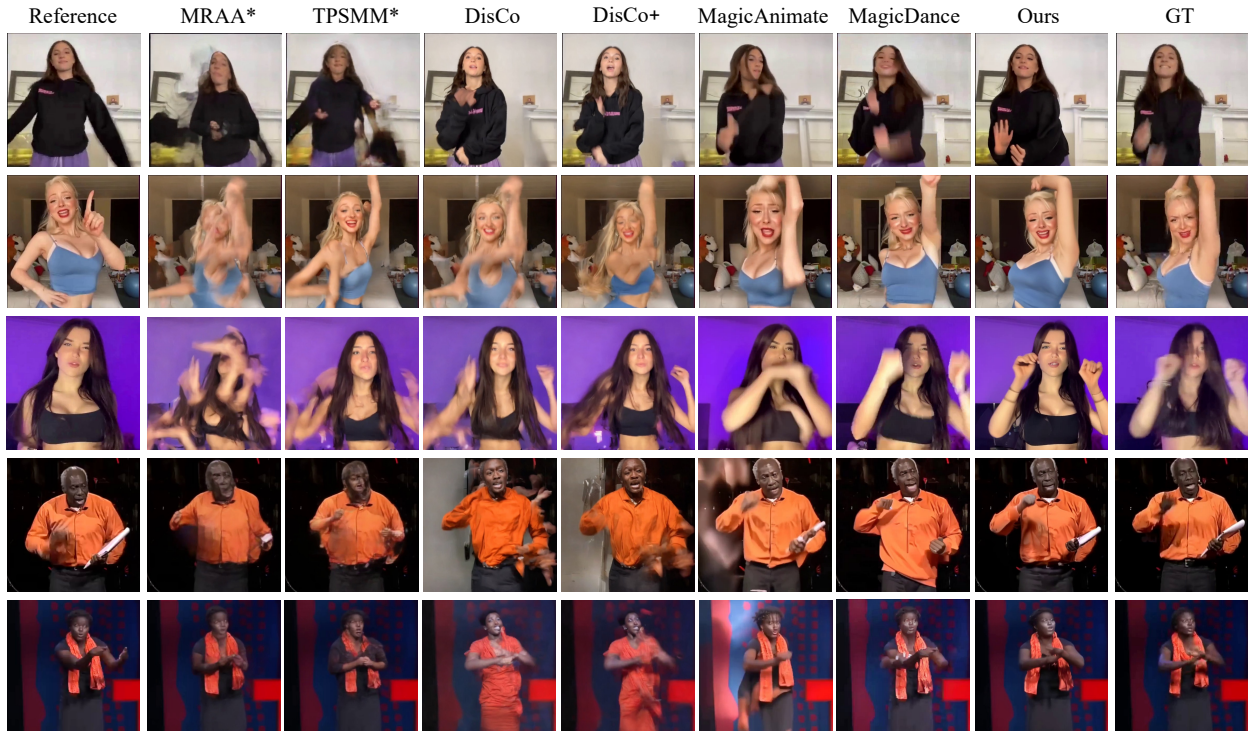


Figure 8: Qualitative comparisons between baselines and our approach on dataset Tiktok (Top three rows) and TED-talks (bottom two rows). MRAA* and TPSMM* present these methods utilizing ground-truth videos as driving signals.

through spatial cross-attention. Meanwhile, the CLIP-encoded reference image is used as the prompt to replace the text prompt in the U-net model. The pose sequence and the aforementioned three conditions are incorporated into the initial noise using the pose guider modules, which are composed of convolutional layers. FYPv2 is formulated as

$$c_{\text{multi}} = c_{\text{pose_seq}} + c_{\text{flow}} + c_{\text{depth}} + c_{\text{ref_pose}}, \quad (10)$$

$$\mathcal{L} = \mathbb{E}_{\mathcal{E}(v_{1:n}, c, \epsilon_{1:n}) \sim \mathcal{N}(0, I), t} [\|\epsilon - \epsilon_{\theta}(z_{1:n}^t, t, x, c_{\text{multi}})\|_2^2], \quad (11)$$

where c_{multi} denotes the overall control condition. The definitions of $v_{1:n}$, $\epsilon_{1:n}$, and $z_{1:n}^t$ are analogous to Eq. (2).

5 EXPERIMENT

5.1 Implementations

Dataset. The robustness of our model to noisy data enables direct training on large unfiltered videos. We collect 4000 character-action videos totaling 2000000 frames as our training set. The data come from public videos on TikTok, YouTube, and other websites. The dataset comprises a diverse range of characters and backgrounds, which facilitates the training of a highly generalizable model.

Training strategy. Our model is trained in two stages. In the first stage, we freeze the weights of VAE [37] and CLIP [28] image encoder, and remove the temporal motion modules. U-Net, ReferenceNet, and multiple-condition guiders are trained to align their spatial generative capacities. In addition, we utilize the weights of Stable Diffusion v1.5 [30] to initialize this training stage. In the

Table 3: Quantitative comparison on Multi-Character Bench. The best and the second-best results are indicated in red and blue respectively.

Method	FID↓	SSIM↑	PSNR↑	FID-VID↓	FVD↓
DisCo[39]	77.61	0.793	29.65	104.57	1367.47
DisCo+[39]	73.21	0.799	29.66	92.26	1303.08
MagicAnime[44]	40.02	0.819	29.01	19.42	223.82
MagicPose[4]	31.06	0.806	31.81	30.95	312.65
Ours	26.95	0.830	31.86	14.56	142.76

second stage, we incorporated temporal motion modules into training along with all parameters from Stage 1, aiming to endow the model with the ability of temporal smoothness. Besides, we use the weights of AnimateDiff v2 [11] to initialize this training stage.

Implementation Details. We sample 16 frames of video, resize and center-crop them to a uniform resolution of 896x640 pixels. Experiments are conducted on 8 NVIDIA A800 GPUs. Both stages are optimized with Adam with a learning rate set to 1×10^{-5} . In the first stage, we train our model for 60k steps with a batch size of 4, and in the second stage, we conduct training for 60k steps with a batch size of 1. At inference, we apply DDIM [34] sampler for 50 denoising steps, with classifier-free guidance [15] scale of 1.5. More details can be found in the appendix.

5.2 Comparisons

Dataset and metrics. Following the previous methods [39], we evaluate our method on TikTok-style videos [39] and TED-talks [33].

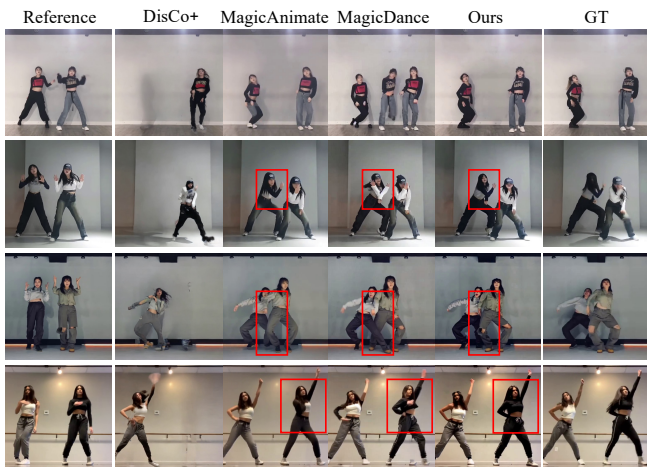


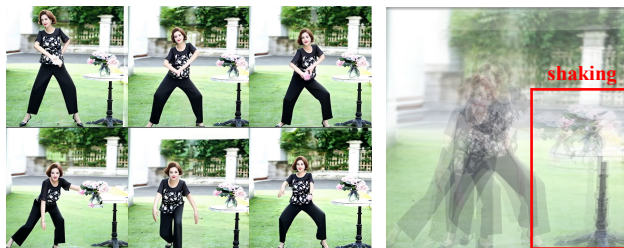
Figure 9: Qualitative comparisons between baselines and our approach on the *Multi-Character* bench.

Table 4: Quantitative ablation results on TikTok Dataset.

Method	FID↓	SSIM↑	PSNR↑	FID-VID↓	FVD↓
w/o Optical Flow	52.94	0.710	28.21	34.35	178.48
w/o Ref. Pose	34.74	0.740	29.13	19.58	139.32
w/o Depth	27.43	0.754	29.98	14.50	119.26
Ours	27.70	0.760	29.70	14.30	117.81

Additionally, due to the lack of benchmarks for multiple-character video generation, we collect 20 multiple-character dancing videos, totaling 3917 frames, from social media, named *Multi-Character*. This dataset serves as a benchmark for evaluating models’ capabilities in generating pose-controllable videos with multiple characters. Our evaluation metrics adhere to the existing research literature [4, 17, 39, 44]. Specifically, we employ conventional image metrics to assess the quality of individual frames, namely L1 error, PSNR [16], SSIM [42], LPIPS [53], and FID [13]. For the video evaluation metric FID-VID [1] and FVD [36], we form a sample by concatenating each consecutive 16 frames.

Baselines. We conduct a comprehensive comparison of our model with several state-of-the-art methods for character animation: (1) MRAA [33] and TPSMM [54] are state-of-the-art GAN-based animation methods. (2) DreamPose [18], Disco [39], MagicAnimate [44], MagicPose [4] and AnimateAnyone [17] are state-of-the-art VLDM-based animation methods. We notice that not all approaches adhere to a uniform generation size. As methods with different generation sizes yield different metrics results, potentially leading to unfair comparisons, we standardize the generation sizes by center-cropping and resizing to 512×512. Under this unified standard, we reevaluate methods that do not conform to this generation size and directly reference relevant statistical data from the original literature of methods that do comply. Note that MRAA [33] and TPSMM [54] utilize ground-truth videos as driving signals but not pose sequences. For fair comparisons, we evaluate two versions using two different driving signals: Visualization of pose sequence and ground-truth videos. As shown in Table 2, MRAA* and TPSMM*



(a) w/o. optical flow condition



(b) w/. optical flow condition

Figure 10: Qualitative comparison results of ablation variants without optical flow condition. Transparent and overlay the images to clearly see the changes in the background.

represent the evaluation metrics using ground-truth videos as driving signals, while MRAA and TPSMM represent the evaluation metrics using visualization of pose sequence as driving signals.

Evaluation on TikTok dataset. Table 1 presents the quantitative comparison experimental results of the comparative methods on the TikTok dataset. Our model outperforms others in state-of-the-art performance on four metrics: SSIM, L1, FID-VID, and FVD, while ranking as the second best on the FID and LPIPS metrics. Notably, our model excels particularly in the realm of video metrics: FID-VID and FVD. Compared with MagicAnimate and AnimateAnyone, the second-best method in FID-VID and FVD, our model showcases a significant improvement of 39% and 35% respectively.

The visual comparison results of the TikTok dataset are shown in the first three rows of Fig. 8. Our approach obtains better performance in pose following and visual quality. The results of the first and third rows showcase the excellent visual quality of our method, which not only accurately follows the pose but also generates hand details that are absent in the ground truth. The second row showcases the powerful pose-following capability of our method, which stands as the sole approach capable of accurately generating the pose with the arm raised in reverse. These results confirm that our approach exhibits superior performance in generating pose-controllable, achieved through training with a large dataset to enhance generalization abilities.

Evaluation on TED-talks dataset. The quantitative comparison results of the TED-talks dataset are depicted in Table 2. Our model achieves sota performance across six evaluation metrics except PSNR, and also demonstrates outstanding performance in the realm of video metrics. In contrast to MagicPose, the second-best of FID-VID and FVD, our model demonstrates a substantial enhancement of 49% and 48% respectively. Note that MRAA* and TPSMM* utilize ground-truth videos as driving signals, thus evaluating perfect yet unfair metrics. Nevertheless, our model manages to surpass or approach them in terms of FID, lpips, FID-VID, and FVD.

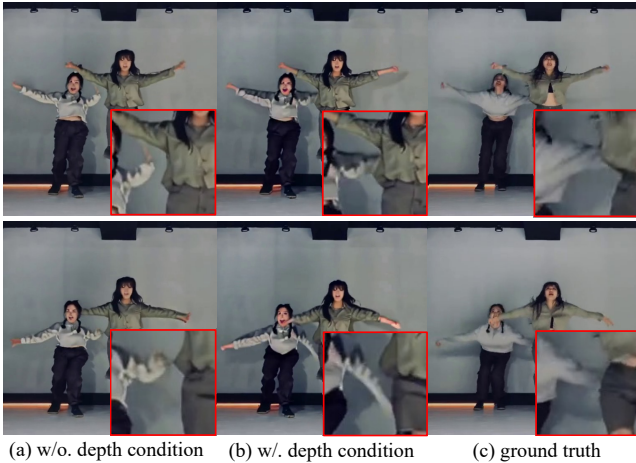


Figure 11: Qualitative comparison results of ablation variants without depth condition.

The last two rows in Fig. 8 illustrate the visual comparison results of the TED-talks dataset. Our approach achieves superior results in pose following and character consistency. In the fourth row, only our results successfully maintain the consistency of the character who holding white notes in the inference image, and in the last row, our results exhibit the best performance in the pose following, while also generating the fewest artifacts.

Evaluation on Multi-Character bench. The quantitative comparison results in Table 3 show that our method significantly outperforms other methods across all metrics on *Multi-Character* bench. In terms of the video metrics FID-VID and FVD, we outperform the second-best method by 25% and 36% in each metric, respectively.

Fig. 9 illustrates the qualitative comparisons between baselines and our approach, highlighting the significant advantages of our approach in maintaining multi-character identity consistency, pose following, and preserving spatial relationships. The top row demonstrates that our approach maintains multi-character identity consistency, whereas other methods fail to do so. As shown in the red boxes on the second and third rows, our approach achieves the most accurate pose following. In the last rows, our approach generates accurate multi-character spatial relationships without occlusion between characters like other methods.

5.3 Ablation Study

To investigate the roles of the proposed conditions, we examine three variants, each without *Optical Flow*, *Depth*, and *Reference Pose*, respectively. Table 4 presents that the proposed full method (“Ours”) with three conditions outperforms other variants in terms of the evaluation metrics. This demonstrates that the three conditions have a positive impact on the model.

Optical Flow. Table 4 presents that the variant without optical flow exhibits the most significant decline, suggesting that optical flow might have the most pronounced positive impact on the model. The comparison results shown in Fig. 10 illustrate where its primary effects are: background stability. In Fig. 10, we overlay the transparent consecutive 6 frames to form the image on the right, enabling a clear depiction of the moving region of this video segment. As indicated by the red boxes, we can observe that the background in the

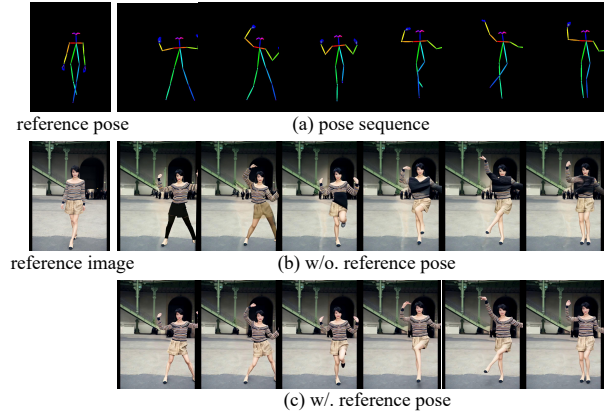


Figure 12: Qualitative comparison results of ablation variants without reference pose condition.

results of the variant without optical flow shows noticeable shaking, whereas the background in the results of the full method with optical flow remains consistently stable. This validates our viewpoint: noisy data with unstable backgrounds leads to the generation of unstable backgrounds by the model, whereas the incorporation of the optical flow condition can solve this problem.

Depth. We conduct a qualitative comparison of multi-character animation in Fig. 11 to validate the positive impact of depth condition. The red boxes highlight the overlapping areas of multiple characters. The variant without depth condition fails to generate the hand of the character on the left placed behind the right character, instead generating a malformed hand. Conversely, the full method with the depth condition can generate overlapping areas of multiple characters. As illustrated by the red boxes in Fig. 11, the hand of the left character is positioned behind the right one, and the hand of the right character is in front of the face of the left one.

Reference Pose. Fig. 12 illustrates the qualitative comparison results when the character position of the inference image and pose sequence are not aligned. The comparison between the variant without reference pose and the full method illustrates that the full method performs better in terms of image quality and character consistency. In the results of the variant, consistency in the background is maintained, yet the clothing of the characters continuously changes, failing to maintain character consistency. In contrast, the full method incorporating the reference pose effectively achieves alignment between character and pose sequence, thereby maintaining character and background consistency.

6 CONCLUSION

In this paper, we propose a pose-controllable character animation framework called *Follow-Your-Pose v2* that integrates multiple conditions into a VLD, dedicated to addressing the issues of background stability and body occlusion of multiple characters. This framework enhances the robustness of the model to noisy data. Within this framework, we design three guiders: optical flow guider, depth guider, and reference pose guider. These guiders effectively address issues of background stability and body occlusion, enhancing the learning of subject appearance. Moreover, we have curated and released a benchmark dataset of pose-controllable videos with multiple characters.

REFERENCES

- [1] Yogesh Balaji, Martin Renqiang Min, Bing Bai, Rama Chellappa, and Hans Peter Graf. 2019. Conditional GAN with Discriminative Filter Generation for Text-to-Video Synthesis. In *International Joint Conference on Artificial Intelligence*. 2.
- [2] Mingdeng Cao, Xintao Wang, Zhongang Qi, Ying Shan, Xiaohu Qie, and Yinqiang Zheng. 2023. MasaCtrl: Tuning-free mutual self-attention control for consistent image synthesis and editing. In *Proceedings of the IEEE/CVF International Conference on Computer Vision*. 22560–22570.
- [3] Caroline Chan, Shiry Ginosar, Tinghui Zhou, and Alexei A Efros. 2019. Everybody dance now. In *Proceedings of the IEEE/CVF International Conference on Computer Vision*. 5933–5942.
- [4] Di Chang, Yichun Shi, Quankai Gao, Jessica Fu, Hongyi Xu, Guoxian Song, Qing Yan, Xiao Yang, and Mohammad Soleymani. 2023. Magicdance: Realistic human dance video generation with motions & facial expressions transfer. *arXiv preprint arXiv:2311.12052* (2023).
- [5] Haoxin Chen, Menghan Xia, Yingqing He, Yong Zhang, Xiaodong Cun, Shaoshu Yang, Jinbo Xing, Yaofang Liu, Qifeng Chen, Xintao Wang, et al. 2023. Videocrafter1: Open diffusion models for high-quality video generation. *arXiv preprint arXiv:2310.19512* (2023).
- [6] Haoxin Chen, Yong Zhang, Xiaodong Cun, Menghan Xia, Xintao Wang, Chao Weng, and Ying Shan. 2024. Videocrafter2: Overcoming data limitations for high-quality video diffusion models. *arXiv preprint arXiv:2401.09047* (2024).
- [7] MMFlow Contributors. 2021. MMFlow: OpenMMLab Optical Flow Toolbox and Benchmark. <https://github.com/open-mmlab/mflow>.
- [8] Patrick Esser, Johnathan Chiu, Parmida Atighehchian, Jonathan Granskog, and Anastasis Germanidis. 2023. Structure and content-guided video synthesis with diffusion models. In *Proceedings of the IEEE/CVF International Conference on Computer Vision*. 7346–7356.
- [9] Riza Alp Güler, Natalia Neverova, and Iasonas Kokkinos. 2018. Densepose: Dense human pose estimation in the wild. In *Proceedings of the IEEE/CVF Conference on Computer Vision and Pattern Recognition*. 7297–7306.
- [10] Xun Guo, Mingwu Zheng, Liang Hou, Yuan Gao, Yufan Deng, Chongyang Ma, Weiming Hu, Zhengjun Zha, Haibin Huang, Pengfei Wan, et al. 2023. I2V-Adapter: A General Image-to-Video Adapter for Video Diffusion Models. *arXiv preprint arXiv:2312.16693* (2023).
- [11] Yuwei Guo, Ceyuan Yang, Anyi Rao, Yaohui Wang, Yu Qiao, Dahua Lin, and Bo Dai. 2023. Animatediff: Animate your personalized text-to-image diffusion models without specific tuning. *arXiv preprint arXiv:2307.04725* (2023).
- [12] Tong He, Yuanlu Xu, Shunsuke Saito, Stefano Soatto, and Tony Tung. 2021. Arch++: Animation-ready clothed human reconstruction revisited. In *Proceedings of the IEEE/CVF International Conference on Computer Vision*. 11046–11056.
- [13] Martin Heusel, Hubert Ramsauer, Thomas Unterthiner, Bernhard Nessler, and Sepp Hochreiter. 2017. Gans trained by a two time-scale update rule converge to a local nash equilibrium. *Advances in Neural Information Processing Systems* (2017).
- [14] Jonathan Ho, Ajay Jain, and Pieter Abbeel. 2020. Denoising diffusion probabilistic models. *Advances in Neural Information Processing Systems* 33 (2020), 6840–6851.
- [15] Jonathan Ho and Tim Salimans. 2022. Classifier-free diffusion guidance. *arXiv preprint arXiv:2207.12598* (2022).
- [16] Alain Hore and Djemel Ziou. 2010. Image quality metrics: PSNR vs. SSIM. In *IEEE International Conference on Pattern Recognition*. 2366–2369.
- [17] Li Hu, Xin Gao, Peng Zhang, Ke Sun, Bang Zhang, and Liefeng Bo. 2023. Animate anyone: Consistent and controllable image-to-video synthesis for character animation. *arXiv preprint arXiv:2311.17117* (2023).
- [18] Johanna Karras, Aleksander Holynski, Ting-Chun Wang, and Ira Kemelmacher-Shlizerman. 2023. Dreampose: Fashion image-to-video synthesis via stable diffusion. In *Proceedings of the IEEE/CVF International Conference on Computer Vision*. IEEE, 22623–22633.
- [19] Levon Khachatryan, Andranik Movsisyan, Vahram Tadevosyan, Roberto Henschel, Zhangyang Wang, Shant Navasardyan, and Humphrey Shi. 2023. Text2video-zero: Text-to-image diffusion models are zero-shot video generators. In *Proceedings of the IEEE/CVF International Conference on Computer Vision*. 15954–15964.
- [20] Diederik P Kingma and Max Welling. 2013. Auto-encoding variational bayes. *arXiv preprint arXiv:1312.6114* (2013).
- [21] Yue Ma, Xiaodong Cun, Yingqing He, Chenyang Qi, Xintao Wang, Ying Shan, Xiu Li, and Qifeng Chen. 2023. MagicStick: Controllable Video Editing via Control Handle Transformations. *arXiv preprint arXiv:2312.03047* (2023).
- [22] Yue Ma, Yingqing He, Xiaodong Cun, Xintao Wang, Siran Chen, Xiu Li, and Qifeng Chen. 2024. Follow your pose: Pose-guided text-to-video generation using pose-free videos. In *Proceedings of the AAAI Conference on Artificial Intelligence*, Vol. 38. 4117–4125.
- [23] Yue Ma, Yingqing He, Hongfa Wang, Andong Wang, Chenyang Qi, Chengfei Cai, Xiu Li, Zhifeng Li, Heung-Yeung Shum, Wei Liu, et al. 2024. Follow-your-click: Open-domain regional image animation via short prompts. *arXiv preprint arXiv:2403.08268* (2024).
- [24] Yue Ma, Hongyu Liu, Hongfa Wang, Heng Pan, Yingqing He, Junkun Yuan, Ailing Zeng, Chengfei Cai, Heung-Yeung Shum, Wei Liu, et al. 2024. Follow-Your-Emoji: Fine-Controllable and Expressive Freestyle Portrait Animation. *arXiv preprint arXiv:2406.01900* (2024).
- [25] Mehdi Mirza and Simon Osindero. 2014. Conditional generative adversarial nets. *arXiv preprint arXiv:1411.1784* (2014).
- [26] Eyal Molad, Eliahu Horwitz, Dani Valevski, Alex Rav Acha, Yossi Matias, Yael Pritch, Yaniv Leviathan, and Yedid Hoshen. 2023. Dreamix: Video diffusion models are general video editors. *arXiv preprint arXiv:2302.01329* (2023).
- [27] William Peebles and Saining Xie. 2023. Scalable diffusion models with transformers. In *Proceedings of the IEEE/CVF International Conference on Computer Vision*. 4195–4205.
- [28] Alec Radford, Jong Wook Kim, Chris Hallacy, Aditya Ramesh, Gabriel Goh, Sandhini Agarwal, Girish Sastry, Amanda Askell, Pamela Mishkin, Jack Clark, et al. 2021. Learning transferable visual models from natural language supervision. In *International Conference on Machine Learning*. 8748–8763.
- [29] Ali Razavi, Aaron Van den Oord, and Oriol Vinyals. 2019. Generating diverse high-fidelity images with vq-vae-2. *Advances in Neural Information Processing Systems* 32 (2019).
- [30] Robin Rombach, Andreas Blattmann, Dominik Lorenz, Patrick Esser, and Björn Ommer. 2022. High-resolution image synthesis with latent diffusion models. In *Proceedings of the IEEE/CVF Conference on Computer Vision and Pattern Recognition*. 10684–10695.
- [31] Olaf Ronneberger, Philipp Fischer, and Thomas Brox. 2015. U-net: Convolutional networks for biomedical image segmentation. In *Medical image computing and computer-assisted intervention—MICCAI 2015: 18th international conference, Munich, Germany, October 5-9, 2015, proceedings, part III 18*. Springer, 234–241.
- [32] Aliaksandr Siarohin, Stéphane Lathuilière, Sergey Tulyakov, Elisa Ricci, and Nicu Sebe. 2019. First order motion model for image animation. *Advances in Neural Information Processing Systems* 32 (2019).
- [33] Aliaksandr Siarohin, Oliver J Woodford, Jian Ren, Menglei Chai, and Sergey Tulyakov. 2021. Motion representations for articulated animation. In *Proceedings of the IEEE/CVF Conference on Computer Vision and Pattern Recognition*. 13653–13662.
- [34] Jiaming Song, Chenlin Meng, and Stefano Ermon. 2020. Denoising diffusion implicit models. *arXiv preprint arXiv:2010.02502* (2020).
- [35] Deqing Sun, Xiaodong Yang, Ming-Yu Liu, and Jan Kautz. 2018. Pwc-net: Cnns for optical flow using pyramid, warping, and cost volume. In *Proceedings of the IEEE/CVF Conference on Computer Vision and Pattern Recognition*. 8934–8943.
- [36] Thomas Unterthiner, Sjoerd Van Steenkiste, Karol Kurach, Raphael Marinier, Marcin Michalski, and Sylvain Gelly. 2018. Towards accurate generative models of video: A new metric & challenges. *arXiv preprint arXiv:1812.01717* (2018).
- [37] Aaron Van Den Oord, Oriol Vinyals, et al. 2017. Neural discrete representation learning. *Advances in Neural Information Processing Systems* 30 (2017).
- [38] Ashish Vaswani, Noam Shazeer, Niki Parmar, Jakob Uszkoreit, Llion Jones, Aidan N Gomez, Lukasz Kaiser, and Illia Polosukhin. 2017. Attention is all you need. *Advances in Neural Information Processing Systems* 30 (2017).
- [39] Tan Wang, Linjie Li, Kevin Lin, Chung-Ching Lin, Zhengyuan Yang, Hanwang Zhang, Zicheng Liu, and Lijuan Wang. 2023. Disco: Disentangled control for referring human dance generation in real world. *arXiv e-prints* (2023), arXiv:2307.
- [40] Ting-Chun Wang, Ming-Yu Liu, Andrew Tao, Guilin Liu, Jan Kautz, and Bryan Catanzaro. 2019. Few-shot video-to-video synthesis. *arXiv preprint arXiv:1910.12713* (2019).
- [41] Ting-Chun Wang, Arun Mallya, and Ming-Yu Liu. 2021. One-shot free-view neural talking-head synthesis for video conferencing. In *Proceedings of the IEEE/CVF Conference on Computer Vision and Pattern Recognition*. 10039–10049.
- [42] Zhou Wang, Alan C Bovik, Hamid R Sheikh, and Eero P Simoncelli. 2004. Image quality assessment: from error visibility to structural similarity. *IEEE Transactions on Image Processing* (2004), 600–612.
- [43] Jay Zhangjie Wu, Yixiao Ge, Xintao Wang, Stan Weixian Lei, Yuchao Gu, Yufei Shi, Wynne Hsu, Ying Shan, Xiaohu Qie, and Mike Zheng Shou. 2023. Tune-a-video: One-shot tuning of image diffusion models for text-to-video generation. In *Proceedings of the IEEE/CVF International Conference on Computer Vision*. 7623–7633.
- [44] Zhongcong Xu, Jianfeng Zhang, Jun Hao Liew, Hanshu Yan, Jia-Wei Liu, Chenxu Zhang, Jiashi Feng, and Mike Zheng Shou. 2023. Magicanimate: Temporally consistent human image animation using diffusion model. *arXiv preprint arXiv:2311.16498* (2023).
- [45] Lihe Yang, Bingyi Kang, Zilong Huang, Xiaogang Xu, Jiashi Feng, and Hengshuang Zhao. 2024. Depth anything: Unleashing the power of large-scale unlabeled data. *arXiv preprint arXiv:2401.10891* (2024).
- [46] Zhendong Yang, Ailing Zeng, Chun Yuan, and Yu Li. 2023. Effective whole-body pose estimation with two-stages distillation. In *Proceedings of the IEEE/CVF International Conference on Computer Vision*. 4210–4220.
- [47] Hu Ye, Jun Zhang, Sibio Liu, Xiao Han, and Wei Yang. 2023. Ip-adapter: Text compatible image prompt adapter for text-to-image diffusion models. *arXiv preprint arXiv:2308.06721* (2023).

- [48] Jae Shin Yoon, Lingjie Liu, Vladislav Golyanik, Kripasindhu Sarkar, Hyun Soo Park, and Christian Theobalt. 2021. Pose-guided human animation from a single image in the wild. In *Proceedings of the IEEE/CVF Conference on Computer Vision and Pattern Recognition*. 15039–15048.
- [49] Wing-Yin Yu, Lai-Man Po, Ray CC Cheung, Yuzhi Zhao, Yu Xue, and Kun Li. 2023. Bidirectionally deformable motion modulation for video-based human pose transfer. In *Proceedings of the IEEE/CVF International Conference on Computer Vision*. 7502–7512.
- [50] Jianfeng Zhang, Hanshu Yan, Zhongcong Xu, Jiashi Feng, and Jun Hao Liew. 2023. Magicavatar: Multimodal avatar generation and animation. *arXiv preprint arXiv:2308.14748* (2023).
- [51] Lvmin Zhang, Anyi Rao, and Maneesh Agrawala. 2023. Adding conditional control to text-to-image diffusion models. In *Proceedings of the IEEE/CVF International Conference on Computer Vision*. 3836–3847.
- [52] Pengze Zhang, Lingxiao Yang, Jian-Huang Lai, and Xiaohua Xie. 2022. Exploring dual-task correlation for pose guided person image generation. In *Proceedings of the IEEE/CVF Conference on Computer Vision and Pattern Recognition*. 7713–7722.
- [53] Richard Zhang, Phillip Isola, Alexei A Efros, Eli Shechtman, and Oliver Wang. 2018. The unreasonable effectiveness of deep features as a perceptual metric. In *Proceedings of the IEEE/CVF Conference on Computer Vision and Pattern Recognition*. 586–595.
- [54] Jian Zhao and Hui Zhang. 2022. Thin-plate spline motion model for image animation. In *Proceedings of the IEEE/CVF Conference on Computer Vision and Pattern Recognition*. 3657–3666.